arXiv:1401.0623v1 [cond-mat.soft] 3 Jan 2014

Magnetic particles confined in a modulated channel: structural transitions tunable by tilting a magnetic field

J. E. Galván-Moya,[1,*] D. Lucena,[1,2] W. P. Ferreira,[2] and F. M. Peeters[1,2,†]

[1] *Department of Physics, University of Antwerp, Groenenborgerlaan 171, B-2020, Antwerp, Belgium*
[2] *Departamento de Física, Universidade Federal do Ceará, Caixa Postal 6030, Campus do Pici, 60455-760 Fortaleza, Ceará, Brazil*

(Dated: January 6, 2014)

The ground state of colloidal magnetic particles in a modulated channel are investigated as function of the tilt angle of an applied magnetic field. The particles are confined by a parabolic potential in the transversal direction while in the axial direction a periodic substrate potential is present. By using Monte Carlo (MC) simulations, we construct a phase diagram for the different crystal structures as a function of the magnetic field orientation, strength of the modulated potential and the commensurability factor of the system. Interestingly, we found first and second order phase transitions between different crystal structures, which can be manipulated by the orientation of the external magnetic field. A re-entrant behavior is found between two- and four-chain configurations, with continuous second order transitions. Novel configurations are found consisting of frozen in solitons. By changing the orientation and/or strength of the magnetic field and/or the strength and the spatial frequency of the periodic substrate potential, the system transits through different phases.

PACS numbers: 82.70.Dd, 52.27.Lw, 64.60.Cn, 81.30.-t

I. INTRODUCTION

Competitive interactions between particles are responsible for the formation of a large variety of complex structures in nature[1–3]. However, to take advantage of this aspect, the major challenge is to find a way to manipulate this formation process, in order to obtain the desired configuration through a correct choice of a set of parameters. Although this idea seems to be promising, there are many other obstacles to overcome.

Formation of Wigner crystals has been widely studied for purely repulsive interaction between particles in quasi-one-dimensional (Q1D)[4–6], two-dimensional (2D)[7, 8] and three-dimensional (3D)[9, 10] systems. These studies showed a very rich set of ground state configurations depending on the system properties, and a diverse kind of transitions was found between them. However, the formation of complex structures increases dramatically when particles interact via competing interaction[11–14]. One of the most simple models is based on the dipole-dipole interaction[15, 16], which can be realized by an external field acting on a system of magnetic particles. The multiple crystalline structures which can be found[17, 18], and the effects of external fields applied on these particles which have been summarized in a recent mini-review[19], indicate the promising future of these kind of systems.

Recent works show the effect of a fixed and oscillating external magnetic field on the crystal structures[20, 21], evidencing that the configuration of the system can be controlled by the orientation of the magnetic field. Numerical works on these systems demonstrated the possibility of cluster formation[22, 23] as well as few-body bound states[24, 25] and local deformations in elongated dipolar gases[26]. Additionally, different transitions between Fermi liquid, solitons and Wigner crystals have been predicted[27, 28] as well as some tunable assemblies[29].

The effect of complex potential landscapes on the structure of interacting colloidal particles was investigated in 1D[30–32] and recently also in 2D[33]. A periodic potential has been proposed to control the arrangement of the particles[13, 33, 34], which is triggered by the commensurability[35, 36] between the periodicity of the potential and the average distance, i.e. the density, of the particles. Experimentally, it was found that a colloidal suspension, where the interaction between particles is negligible, exhibits a non-trivial dependence on the strength of the modulated potential[37]. This finding allows the possibility to use the modulated potential as an effective tunable parameter for a system of interacting particles.

In the present work the ground state configuration of a system of magnetic particles confined by a parabolic Q1D channel on a periodic substrate potential is studied. Magnetic particles are aligned with an external tilted magnetic field and interacting through an anisotropic dipole-dipole potential[15], which depends on the orientation of the external field. We investigate how the orientation of the field allows to tune the ground state configuration of the system, modulating the competitive interaction between each pair of particles. The effect of the modulated potential is analyzed through its strength and the degree of commensurability of the system imposed by the periodicity of the substrate potential and the average inter-particle distance, i.e. the density.

The present paper is organized as follows. In Sec. II the model system and the numerical methods are de-

* Email: JesusEduardo.GalvanMoya@uantwerpen.be
† Email: Francois.Peeters@uantwerpen.be

scribed. In Sec. III we present the results for the different ground state transitions of the commensurate system, and the tuning between the different phases is realized by changing the orientation of the magnetic field and the external modulated potential. In sect. IV the same analysis is presented for a non-commensurate system, and the effects due to the commensurability factor are explained. Our conclusions are given in Sec. V.

II. MODEL SYSTEM

In this work, we consider a system of N identical interacting magnetic particles, which are allowed to move in the $x-y$ plane. The magnetic particles are confined by an external parabolic potential in the y direction and a periodic substrate potential along the x direction with period length L and potential height V.

The system is subjected to an external and spatially homogeneous magnetic field $\mathbf{B}$, which induces a magnetic moment $\boldsymbol{\mu}$ to all particles, aligning them to $\mathbf{B}$. The magnetic field is tilted by an angle θ with respect to the z-axis, which is perpendicular to the plane of motion, and it forms an angle φ with respect to the x-axis of the plane. This is schematically represented in Fig. 1.

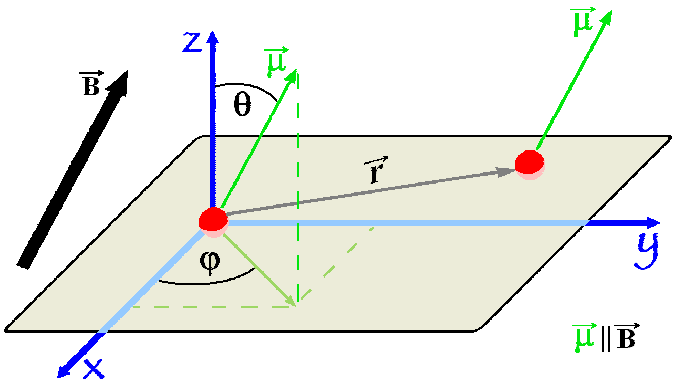

FIG. 1. (Color online) Schematic representation of two dipolar particles (red spheres). All particles are confined to the $x-y$ plane and the magnetic moment $\boldsymbol{\mu}$ of each one is aligned to the external magnetic field $\mathbf{B}$.

At short distances the interaction between the colloidal particles is a hard-core repulsion which defines the characteristic length (the diameter of each particle - σ) and the energy scale (ε) of the system. The total energy of the system is given by

$$H = \sum_{i=1}^{N}\left[\frac{1}{2}m\omega_0^2 y_i^2 - V\cos\left(\frac{2\pi x_i}{L}\right)\right] + \sum_{i=1}^{N}\sum_{j>i}^{N}\left[4\varepsilon\left(\frac{\sigma}{|\mathbf{r}_{ij}|}\right)^{12} + V_{dip}(\mathbf{r}_{ij},\boldsymbol{\mu})\right], \quad (1)$$

where $\mathbf{r}_{ij} = x_{ij}\hat{\mathbf{e}}_\mathbf{x} + y_{ij}\hat{\mathbf{e}}_\mathbf{y}$ represents the relative position between the i-th and the j-th particle and $V_{dip}(\mathbf{r}_{ij},\boldsymbol{\mu})$ is the dipole-dipole interaction[15, 16, 24] given by

$$V_{dip}(\mathbf{r}_{ij},\boldsymbol{\mu}) = \frac{1}{r_{ij}^5}\left[(\mu r_{ij})^2 - 3(\boldsymbol{\mu}\cdot\mathbf{r}_{ij})^2\right], \quad (2)$$

where we assume that the magnetic moment of each particle $\boldsymbol{\mu}$ is aligned to $\mathbf{B}$. Equation (2) can be rewritten as follows

$$V_{dip}(\mathbf{r}_{ij},\theta,\varphi) = \frac{\mu^2(1-3\sin^2\theta\sin^2(\varphi))}{|\mathbf{r}_{ij}|^3} - \frac{3\mu^2\sin^2\theta}{|\mathbf{r}_{ij}|^5}x_{ij}\left(\cos(2\varphi)x_{ij} - \sin(2\varphi)y_{ij}\right). \quad (3)$$

A contour plot of the pairwise interaction of Eq. (3), is shown in Fig. 2 as a function of the relative x and y distances between two particles for different values of θ, as specified in the figures, with fixed φ. The anisotropy of the dipole-dipole interaction (see Fig. 2), plays an important role in the determination of the many-particle ground-state configuration, as it will be discussed later, breaking the widely studied chain-like structure found for systems with isotropic pairwise interaction[4–6]. The anisotropy of the interaction is governed by the angles θ and φ, nevertheless, as shown in this work, the strength of the periodic potential can overcome the effect of the anisotropy, determining the many-particle configuration.

In dimensionless units, the total energy of Eq. (1) becomes

$$H = \sum_{i=1}^{N}\left[\upsilon^2 y_i^2 - V_0\cos\left(\frac{2\pi x_i}{L}\right) + \sum_{j>i}^{N}\left\{\frac{4}{|\mathbf{r}_{ij}|^{12}} + \frac{\mu^2(1-3\sin^2\theta\sin^2(\varphi))}{|\mathbf{r}_{ij}|^3} - \frac{3\mu^2\sin^2\theta}{|\mathbf{r}_{ij}|^5}x_{ij}\left(\cos(2\varphi)x_{ij} - \sin(2\varphi)y_{ij}\right)\right\}\right], \quad (4)$$

where the energy and the distances are given in units of ε and σ, respectively. The dimensionless confinement frequency is defined by $\upsilon^2 = m\omega_0^2/2\varepsilon\sigma^2$ and the dimensionless strength of the substrate potential by $V_0 = V/\varepsilon$, while the dimensionless magnetic moment of each particle can be redefined by $\boldsymbol{\mu}/\varepsilon\sigma^3 \Rightarrow \boldsymbol{\mu}$.

We introduce the dimensionless linear density η and the periodicity number n, defined respectively as the number of particles and the number of periods of the periodic potential per unit length along the x direction. The presence of the periodic potential leads to the commensurability factor[35]

$$p = \frac{N}{n} = \eta L, \quad (5)$$

expressing the commensurability between the period L and the average distance between the particles.

In order to characterize the system, we define three different states of commensurability. *i)* S_I: when $p \in \mathbb{Z}$, which is a commensurate state; *ii)* S_{II}: when $p = k/m$: $k \in \mathbb{Z}$, $m \in \mathbb{N}$, $k \neq m$, it means that the system is

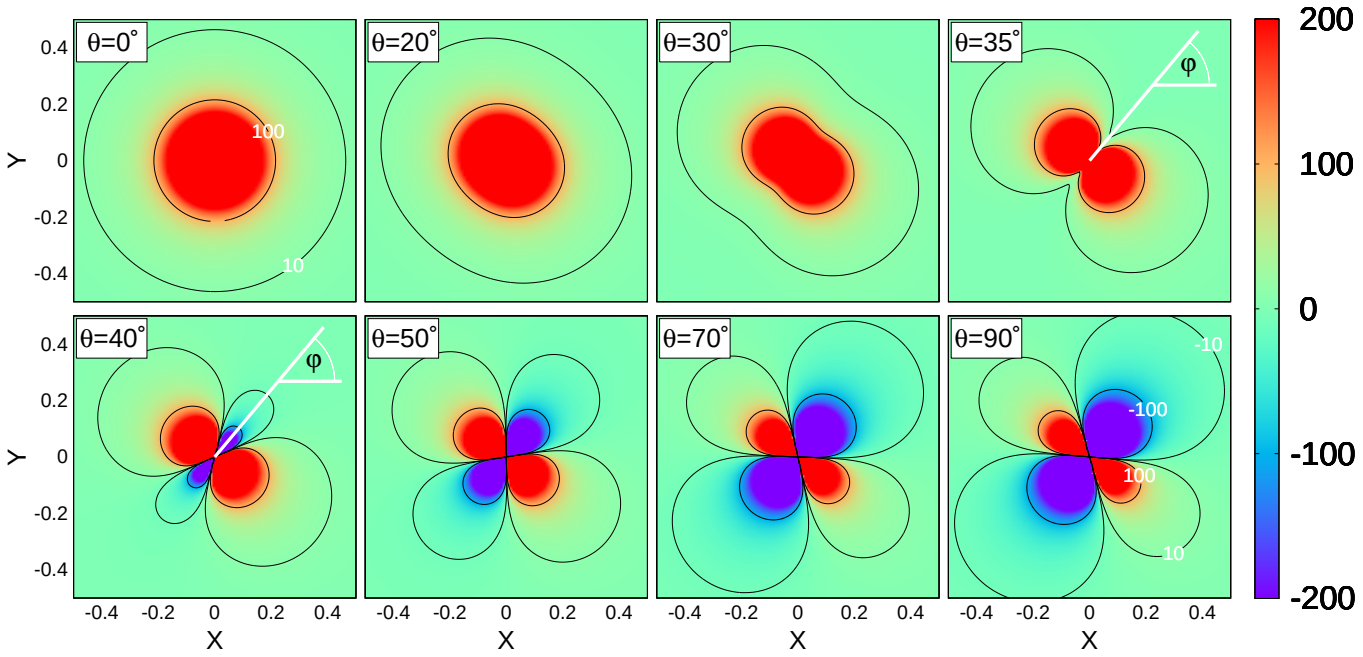

FIG. 2. (Color online) The dipole-dipole interaction as a function of the relative (x,y)-position between two particles, is plotted for different values of the angle θ between the magnetic field and the z-axis. The value of θ is specified in the figures, while the strength of the interaction is indicated by the color bar. The contour lines are plotted for different values of the interaction energy, as labeled in the first and last figures. The direction of $\mathbf{B}$ in the $x-y$ plane is indicated by the angle φ in the top right figure.

not completely commensurate, this state could be subdivided into S_{II}^{-} for $p<1$ and S_{II}^{+} for $p>1$; *iii*) S_{III}: when $p\in\{\mathbb{R}-\mathbb{Q}\}$ and it implies that the system is incommensurate. In this work we will limit our analysis to systems belonging to the first two categories.

We investigate the ground state configuration of the system, using Monte Carlo simulations (MC) optimized with the Newton method, which has been previously used to analyze the structural transitions in Q1D systems with purely repulsive interaction[4–6, 38]. For all numerical results of the present work we consider $\upsilon=1$ and $\mu=1$.

We will study the dependence of the ground state configurations on the orientation of the magnetic field. For that, we fix the linear density of the system to the value $\eta=0.8$. Previously[4, 5, 38] it was shown for $\mathbf{B}$ perpendicular to the $x-y$ plane, the dipoles are no longer arranged in a single-chain configuration at the center of the parabolic channel for $\eta=0.8$, but split in a two-chain configuration. The effect of the magnetic field strength will not be studied, since we are considering a system with superparamagnetic dipole particles, (i.e. the magnetic moment of all particles is aligned along $\mathbf{B}$).

III. COMMENSURATE SYSTEM ($p=1$)

For a typical commensurate state ($p=1$), the anisotropy of the system is strongly determined by the direction of $\mathbf{B}$. In order to understand this effect, Fig. 3 shows the phase diagram of the system as a function of the planar (φ) and azimuthal (θ) angles of the direction of $\mathbf{B}$, when the strength of the periodic potential is $V_0=0.03$. In this diagram the solid and dashed curves represent first and second order phase transitions, respectively.

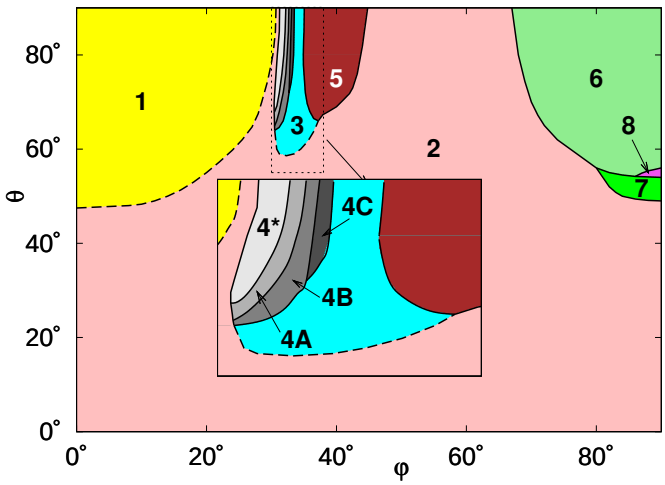

FIG. 3. (Color online) Phase diagram of the ground state configuration, for a system of dipole particles in the regime S_I with $p=1$ and $V_0=0.03$. The solid (dashed) lines represent first (second) order transitions. Numbered phases are shown in Fig. 4.

In Fig. 4 we present the ground state configurations

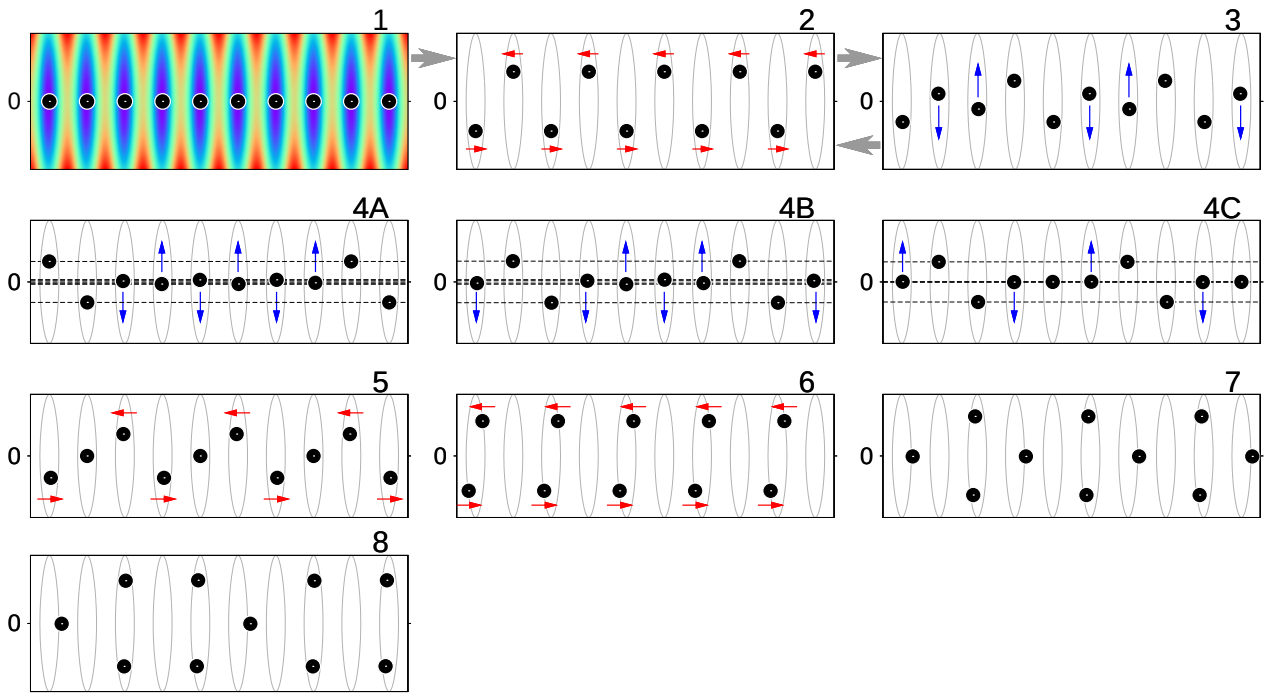

FIG. 4. (Color online) Different ground state configurations found for the system with $p = 1$. The small red (blue) arrows show the movement of the particles in each phase caused by a small increment of φ (V_0), while the gray ellipses represent the cells formed by the confining and periodic potentials (which is plotted as a color contour plot in 1).

as they are numbered in the phase diagram (see Fig. 3). The small red and blue arrows indicate the displacement of the particles when increasing φ and V_0, respectively, while the gray arrows between two configurations indicate that the transition between them occurs continuously.

From Fig. 4 one can see that, until phase 5, all ground state configurations follow the following rule: one particle per one cell (we call cells the wells formed by the total confinement potential which are marked in Fig. 4 by gray ellipses). However, with the exception of phase 1, when increasing φ most of the particles move away from the center of the cell due to the anisotropic inter-particle interaction, following the directions shown by the red arrows.

A. Transition from isotropy to anisotropy interaction

From Eq. (3) we notice that for $\theta = 0°$ the interaction between particles is purely repulsive and is given by $V_{dip}(r) = \mu^2/r^3$. As was found in Refs. [4,5,38], the ground state of the system is given by a zigzag configuration, which is represented by phase 2. Notice also from Fig. 3, that for $\theta = 0°$ the ground state is a zigzag configuration irrespective of the value of φ, evidencing the isotropy of the inter-particle interaction.

The anisotropy of the interaction arises slowly by increasing θ, resulting in a lowering of the lowest eigenfrequency of the system for small φ and it slowly increases with φ as seen in Fig. 5. Taking into account that the stability of a configuration is directly related to the value of its lowest eigenfrequency, we notice, that as an effect of the anisotropy of the pairwise interaction, the stability of the two-chain configuration (phase 2 in Fig. 4) in-

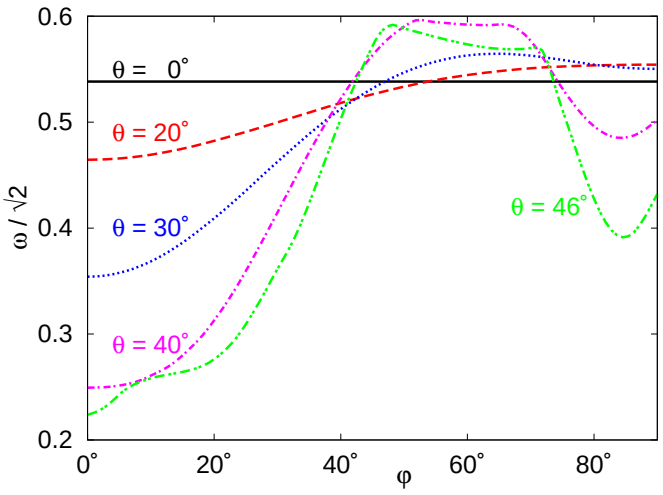

FIG. 5. (Color online) Lowest eigenfrequency of the two-chain configuration (phase 2) as a function of the planar angle (φ) for different values of θ. The other parameters are $p = 1$ and $V_0 = 0.03$.

creases for intermediate values of φ ($45° \lesssim \varphi \lesssim 70°$) by increasing θ, while the opposite behaviour was found for $\theta \lesssim 30°$.

From Fig. 3 one can see that for $\theta \gtrsim 47°$ the anisotropy of the pairwise interaction introduces new phases as ground state, now depending on φ. The very rich variety of phases produces in most of the cases first order transitions between them, as is evidenced in Fig. 6, through the discontinuous jumps in the lowest eigenfrequency of the system.

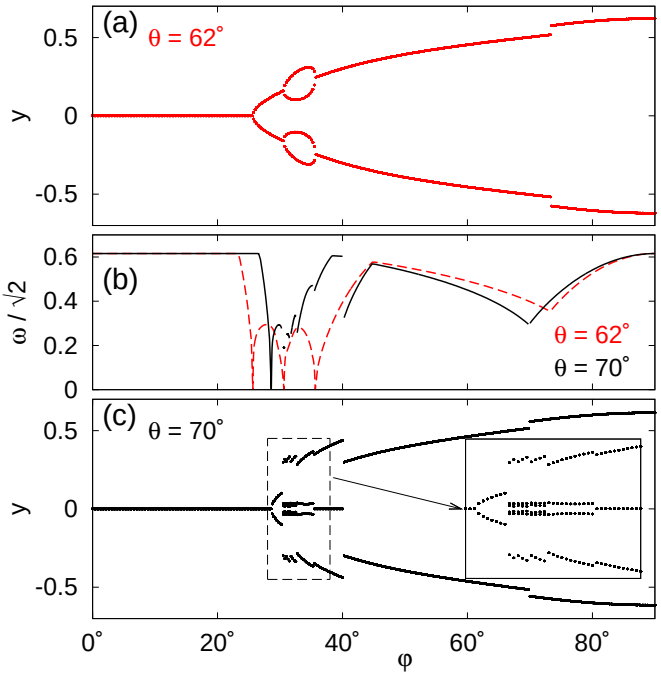

FIG. 6. (Color online) (a), (c) The y-position of the particles in the ground state for a system with $p = 1$ and $V_0 = 0.03$ as a function of φ, for two different values of θ indicated in each figure. (b) Lowest eigenfrequency of the system. Structural transitions occur when ω exhibits a jump (first order) or when it becomes zero (second order).

The transition between the single- and the two-chain (phase 2) configuration (zigzag transition) appears in the region where the dipole-dipole interaction is dominantly attractive. For $\theta \gtrsim 47°$, the single-chain configuration (phase 1) is the ground state for small values of φ and this region increases with increasing θ. The continuous transition between these two phases in the y-direction, is shown in Fig. 6(a), while Fig. 6(b) shows that the lowest eigenfrequency goes to zero which is the evidence of a second order phase transition[4].

B. Transition between $2-4-2$ chains: Re-entrant behavior

A second order transition in the ground state configuration occurs between phases 2 and 4 (Fig. 4). Such a transition reveals an interesting effect which is put in evidence in Fig. 6(a). The transition between $2-4-2$ chains is found by increasing φ within the interval ($59° \lesssim \theta \lesssim 63°$) in the $\theta - \varphi$ phase diagram (Fig. 3). This is demonstrated in Fig. 6(a) for $\theta = 62°$. A similar re-entrant process has been found in dipolar fluids[39] and recently also for Q1D systems of patchy particles[40, 41] and ferrogels[42].

This re-entrant process occurs after the zigzag transition takes place. In Fig. 6(b) we show that, by increasing φ, the two-chain configuration (phase 2) becomes less stable, since its lowest frequency approaches zero at the point where the four-chain configuration (phase 3) arises from a continuous lattice deformation of phase 2. After that, the stability of the four-chain configuration increases until $\varphi \simeq 33°$, where the lowest eigenfrequency starts to decrease, returning to the two-chain configuration through a continuous deformation of the lattice. During this process the lowest eigenfrequency of phase 3 decreases to zero, after that phase 2 appears again through a second order transition (Fig. 6(b)).

The mechanism of this re-entrant process, which occurs through a continuous deformation of the lattice, is outlined in Fig. 7. Notice that this re-entrant process is qualitatively different from the one found earlier in Ref. 4, where these processes were found to be of first order. This difference is due to the presence of the periodic potential. Without the periodic potential the particles not only undergo a zigzag transition, but they also exhibit a discontinuous shift in the x-direction which now is prevented by the periodic potential.

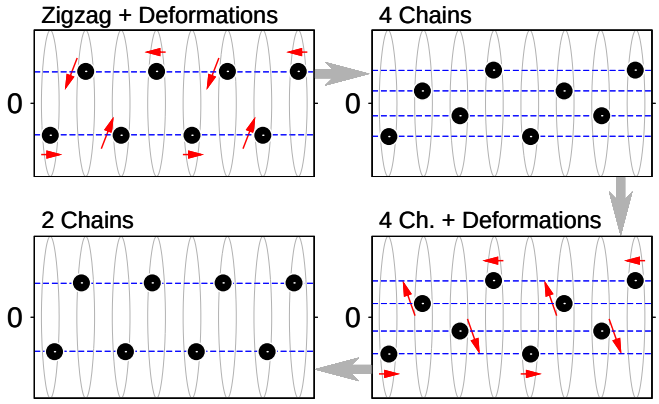

FIG. 7. (Color online) Mechanism of the re-entrant process between $2-4-2$ chains in the system. The horizontal dashed lines accentuate the chain-like configuration of each phase.

C. Soliton-like deformations of the single-chain phase

For larger values of θ ($\theta \gtrsim 70°$) the anisotropy of the dipole-dipole interaction determines most of the transitions found for the ground state configurations. It forces to align the particles along $\mathbf{B}$ forming (short) row-like ar-

rangements, which may even result in the localization of two particles in the same cell of the periodic potential, as shown in Fig. 3 for $V_0 = 0.03$ (e.g., see phases 2, 5 and 6). Some of these transitions result in a sequential deformation of the single-chain configuration as shown in the highlighted region in Fig. 6(c), where the y-position of the particles is plotted as a function of φ for $\theta = 70°$. In this case the deformations appear between the two- and four-chain configurations, and the region between the phases is identified in the phase diagram (Fig. 3) as phase 4.

In Fig. 6(c) one can observe that, by increasing φ, the ground state phase transitions in the highlighted region are a sequence of single-chain and two-chain configurations followed by a group of disorder-like phases and after that four- and three-chain configurations, where all transitions are of first order with the exception of the zigzag transition which has been previously analyzed. The first order transitions are evidenced by the discontinuities in the lowest eigenfrequency of the system[4, 6] and the jumps in the y-coordinate position.

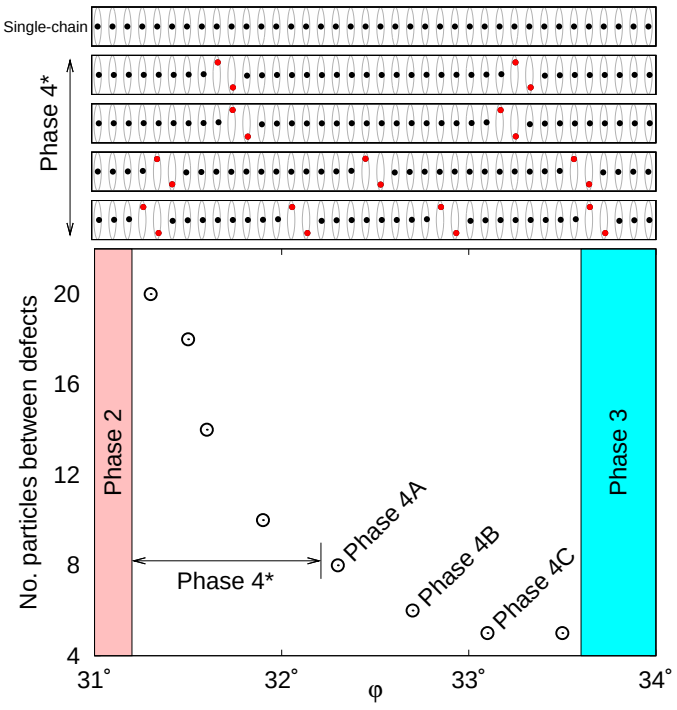

FIG. 8. (Color online) The number of particles between defects (i.e. solitons) during the single-chain sequential deformation process, is plotted as a function of φ for $\theta = 90°$ and $V_0 = 0.03$. Configurations of the disordered phases are shown in the upper figures, where the positions of the defects are highlighted by red symbols for the particles, and the gray ellipses indicate the cells formed by the confinement in combination with the periodic potential.

The disorder-like phases aforementioned are a consequence of the high anisotropy of the interaction potential. In order to understand this effect we consider the limiting case $\theta = 90°$, where the dipole-dipole interaction is dominantly attractive for $\varphi < 30°$. In this limit the competition between the inter-particle interaction and the periodic confinement potential ($V_0 = 0.03$) produces a deformation of the single-chain configuration immediately after the two-chain configuration appears. The single-chain configuration is suddenly broken by a local deformation of the lattice, after that, the period of the position where such a deformation occurs decreases with φ until the four-chain configuration (phase 3) is reached.

In the upper part of Fig. 8 we show the deformation process presenting some configurations that are typical for phase 4*. In those configurations the location of the defects are marked with red symbols for the particles. They appear as frozen solitons whose density increases with φ. From those configurations, the deformation process can be understood as a perturbation on the one-dimensional lattice, uniformly distributed on the axial direction, which allows that the system evolutes through first order transitions, into a Wigner crystalline structure. In order to clarify this process, we plot the number of particles between defects (or solitons) as a function of φ for the largest anisotropy of the interaction between particles (i.e. $\theta = 90°$) when $V_0 = 0.03$, in Fig. 8. This figure shows how the spatial frequency of the defects (or the density of solitons) increases by increasing φ, reducing the number of particles between defects until the ground state structure reaches the four-chain configuration (phase 3). This process has been found previously for an infinite system of particles interacting through a purely repulsive interaction, confined by a power-law potential y^α when $\alpha < 2$, by increasing the linear density of the system[5].

D. Effect of the periodic substrate potential

In this section we pay attention to the effect of the substrate potential on the ground state configuration in the commensurate case with $p = 1$ and $\theta = 90°$. The ground state configurations are summarized in the $V_0 - \varphi$ diagram which is presented in Fig. 9. Notice that for $\theta = 90°$ the anisotropy of the dipole-dipole interaction is maximum (see Fig. 2). For some intervals of φ (e.g. $\varphi \lesssim 30°$, $\varphi \gtrsim 68°$) the ground state configuration is unaffected by V_0. For $\varphi \lesssim 30°$ the dipole-dipole interaction along the x-axis is dominantly attractive and the single-chain configuration is found as the ground state (Fig. 4). On the other hand, for $\varphi \gtrsim 60°$ the dipole-dipole interaction along the x-axis becomes dominantly repulsive and the two-chain configuration is now obtained as the ground state which is independent of V_0. There is an intermediate interval $30° \lesssim \varphi \lesssim 68°$ in which it is possible to control the system configuration through the strength of the substrate V_0.

The process of the single-chain sequential deformation, as previously discussed, is attenuated by increasing V_0 reducing this process to a very narrow region (see inset in Fig. 9), where the deformation is reduced to the phases $4A - 4C$. For $V_0 > 1$ the ground state configuration is

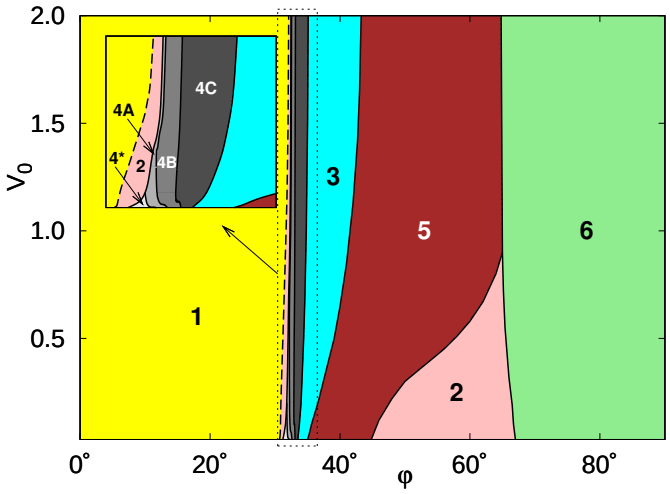

FIG. 9. (Color online) Phase diagram of the ground state configuration, for a system of dipole particles for the case S_I with $p = 1$ and $\theta = 90°$. Different phases are plotted in different colors as a function of the angle φ and the strength of the substrate potential V_0. The solid (dashed) lines represent first (second) order transitions between the phases. Numbered phases are shown in Fig. 4. The dashed box area is enlarged in the inset.

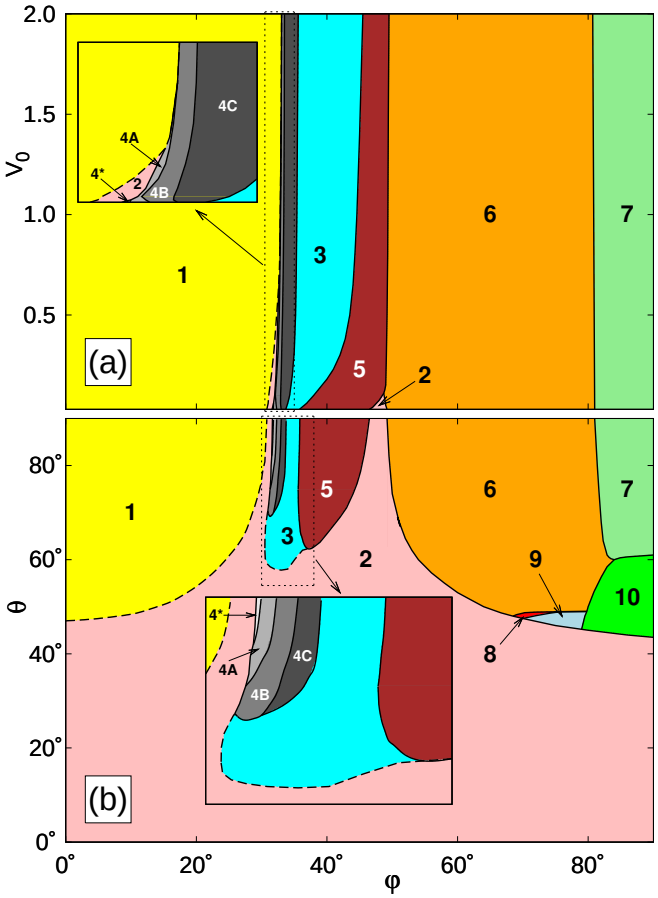

FIG. 10. (Color online) Phase diagram of the ground state configuration for a system of dipole particles in the regime S_{II} with $p = 1/2$. Different phases are plotted as a function of (a) φ and V_0 for $\theta = 90°$, and (b) φ and θ for $V_0 = 0.03$. The solid (dashed) lines represent first (second) order transitions between phases. Numbered phases are shown in Fig. 11. The dashed box areas are elongated in the insets.

less sensitive to a variation of V_0, as is visible in Fig. 9. In all cases the effect of V_0 is to rearrange the configuration by moving the particles towards the center of the cell in the y-direction, as was previously studied in Ref. [32].

It is interesting to note that phases 7 and 8 do not appear in Fig. 9, showing that these are characteristic configurations produced by the anisotropy of the interaction, which can be found in a small window of the angles θ and φ, for a weak strength of the periodic potential V_0, as shown in Fig. 3. The configuration of these phases (see Fig. 4) is evidence that the position of the particles are mainly determined by the interaction potential.

IV. NON-COMPLETELY COMMENSURATE SYSTEM ($p = 1/2$)

We further analyze the influence of the commensurability factor on the system by taking $p = 1/2$ bearing in mind that p can be controlled by L or the linear density η (see Eq. (5)). The ground state configurations are summarized in the $V_0 - \varphi$ ($\theta - \varphi$) phase diagram for $\theta = 90°$ ($V_0 = 0.03$) which is presented in Fig. 10(a) (10(b)). The configurations of the numbered phases in Fig. 10 are shown in Fig. 11, where the gray ellipses indicate the cells formed by the confinement and the periodic potential.

From Fig. 10(a), one can see that the effect of the periodic potential increases with increasing V_0, as was studied in previous section, and it results in a rearrangement of the configuration, moving the particles towards the center of the cell. The single-chain sequential deformation process described by phases 4^* and $4A - 4C$ which were analyzed in Sec. III C, is still present for $p = 1/2$. However, due to the existence of an empty cell between two nearest particles in these phases (see Fig. 11), the movement in the x-direction is highly restricted, as a consequence the single-chain deformation process will be reduced rapidly to the phases $4B$ and $4C$ by increasing V_0, as is shown by the inset in Fig. 10(a). In the same way, the zigzag transition disappears around $V_0 = 0.5$, allowing the system to transit from phase 1 directly to phase 4 for higher values of V_0.

On the other hand, Fig. 10(b) shows that due to the symmetry of the periodic potential wells, the effect of the interaction anisotropy on the system for small values of θ, is similar to the previously discussed case of $p = 1$ allowing to make the two-chain configuration (phase 2 in Fig. 11) as the ground state. Additionally, by increasing θ the stability of phase 2 decreases allowing the system to reach other configurations as ground state. After that, several phases are found, but only until phase 5 the ground state configurations correspond to one parti-

cle per two cells, showing the large influence of p on the system inside the region $\varphi < 50°$.

As a consequence of the new symmetry imposed by the commensurability factor some new configurations, beyond those found for the case $p = 1$, are found for the case $p = 1/2$. As was discussed at the end of previous section, these configurations (phases 6, 8 and 9) are generated as a consequence of the anisotropy of the interaction potential for intermediate values of θ.

Figs. 12(a,b) show an interesting transition in the region $60° \lesssim \varphi \lesssim 80°$ for $\theta = 48°$ and $V_0 = 0.03$. In this region the ground state changes between phases $2-6-8-9-10$, where the first two correspond to different two-chain configurations, and the last one is a typical Q1D Wigner crystal with a three-chain configuration. Nevertheless, transition between phase 8 (eight chains) and phase 9 (ten chains) occurs with a small discontinuity in its lowest eigenfrequency as shown in Fig. 12(b) around $\varphi = 71°$. Such a transition is even more clear in Fig. 12(a) where the y-position of the particles are plotted as a function of φ. In Fig. 11, the configuration of phases 8 and 9 are shown where the dashed lines indicate the position of the different chains. Additionally, the red arrows show the displacement of the particles when φ increases.

The two-chain configuration for $p = 1/2$ is found in three different phases (2, 6 and 7 in Fig. 11), which shows that the zigzag symmetry is broken with increasing φ. However, the transition between these phases is discontinuous, even for small values of V_0, as shown in Fig. 12(b) for $\theta = 66°$ and $V_0 = 0.03$, where the discontinuities in the lowest eigenfrequency of the system indicate first order transitions between these phases. These discontinuities are also evident in the y-position of the particles as a function of φ in Fig. 12(c).

V. CONCLUSIONS

We studied a Q1D system of magnetic particles confined by a parabolic channel modulated by a periodic substrate potential, where the magnetic moment of all particles is aligned by an external tilted magnetic field. The linear density in the direction of the modulated potential was fixed to $\eta = 0.8$ and the ground state configuration at zero temperature was analyzed as a function of the magnetic field orientation, strength of the periodic potential and commensurability factor. A plethora of different particle configurations are found as ground state, which are arranged in a different number of chains, and we even found a remarkable soliton-like configuration where the density of solitons could be varied with the tilt angle.

The anisotropy of the pairwise interaction between particles, determined by the magnetic tilt angles θ and φ is largely responsible for the crystalline configuration of the system, but its effect decreases by increasing V_0. For small values of V_0, the angle θ controls the degree of anisotropy of the system and with the in-plane angle φ it is possible to tune the ground state configuration. On the other hand, for the limiting case of maximum pairwise anisotropy ($\theta = 90°$), the control of the ground state configuration depends weakly on φ for large values of V_0.

The commensurability factor not only changes the stability region of the phases, as shown in the phase diagrams, but it also produces the emergence of characteristic ground state configurations due to its symmetry. However, in order to get these characteristic phases for each commensurability factor, it is necessary to tune θ and φ to appropriate values.

From these results we can conclude that varying θ and φ allows us to tune the ground state of the system, while the effect of V_0 is to rearrange the configuration by moving the particles to the center of the cells in the y direction. The commensurability factor, controlled by L or the density, acts as a complementary tunable parameter which gives the freedom to build a desired configuration. This could be very useful as input parameter for experiments with magnetic particles, where the sinusoidal confinement can be realized by the application of external potentials through spatially varying light field, which have been used to induce structural changes in colloidal systems[13, 30, 43], while the configurations can be obtained by video microscopy for different external magnetic fields as was demonstrated in Ref. 16.

ACKNOWLEDGMENTS

This work was supported by the Flemish Science Foundation (FWO-Vl), the Methusalem programme of the Flemish government, CNPq, CAPES, FUNCAP (Pronex grant), the collaborative program CNPq - FWO-Vl and the Brazilian program Science Without Borders CsF. Computational resources were provided by HPC infrastructure of University of Antwerp (CalcUA) a division of the Flemish Supercomputer Center (VSC).

[1] E. V. Shevchenko, D. V. Talapin, N. A. Kotov, S. O'Brien, and C. B. Murray, Nature **439**, 55 (2006).
[2] Y. Min, M. Akbulut, K. Kristiansen, Y. Golan, and J. Israelachvili, Nat. Mater. **7**, 527 (2008).
[3] R. M. Choueiri, A. Klinkova, H. Thérien-Aubin, and M. Rubinstein, J. Am. Chem. Soc. **135**, 10262 (2013).
[4] G. Piacente, I. V. Schweigert, J. J. Betouras, and F. M. Peeters, Phys. Rev. B **69**, 045324 (2004).
[5] J. E. Galván-Moya and F. M. Peeters, Phys. Rev. B **84**, 134106 (2011).
[6] J. E. Galván-Moya, K. Nelissen, and F. M. Peeters, Phys. Rev. B **86**, 184102 (2012).

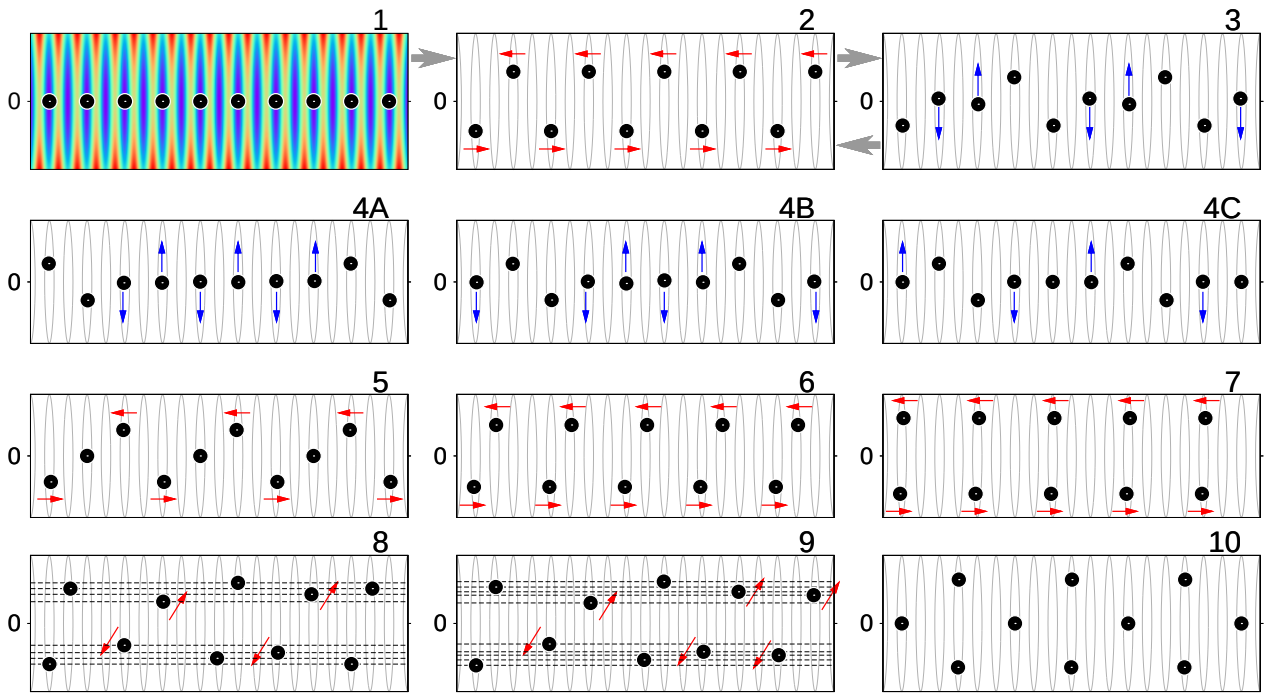

FIG. 11. (Color online) Different ground state configurations found for the system with $p = 1/2$. The small red (blue) arrows show the movement of the particles in each phase caused by a small increment of φ (V_0), while the gray ellipses represent the cells formed by the confining and periodic potentials (which is plotted as a color contour plot in 1).

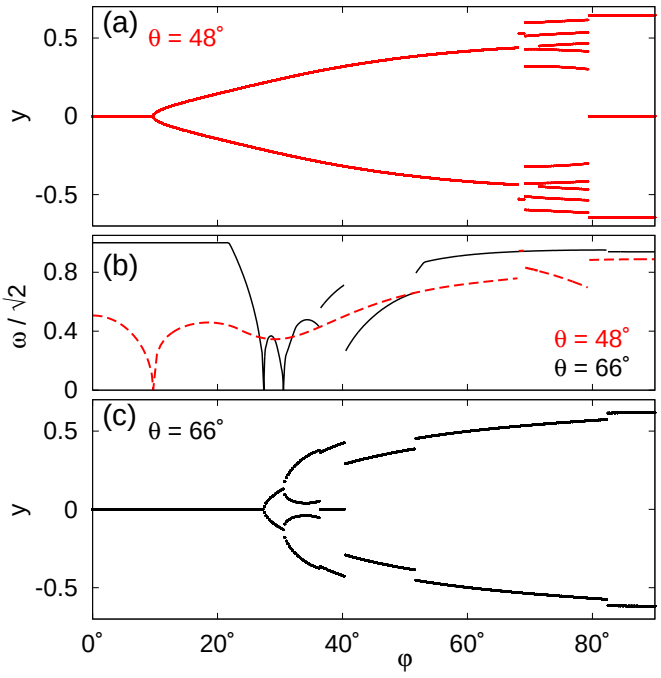

FIG. 12. (Color online) (a), (c) The y-position of the particles in the ground state for a system with $p = 1/2$ and $V_0 = 0.03$ as a function of φ, for two different values of θ indicated in each figure. (b) Lowest eigenfrequency of the system.

[7] V. A. Schweigert and F. M. Peeters, Phys. Rev. B **51**, 7700 (1995).
[8] B. Partoens, V. A. Schweigert, and F. M. Peeters, Phys. Rev. Lett. **79**, 3990 (1997).
[9] R. W. Hasse and V. V. Avilov, Phys. Rev. A **44**, 4506 (1991).
[10] Y. G. Cornelissens, B. Partoens, and F. M. Peeters, Physica E **8**, 314 (2000).
[11] C. O. Reichhardt, C. Reichhardt, and A. Bishop, Phys. rev. Lett. **92**, 016801 (2004).
[12] Y. H. Liu, L. Y. Chew, and M. Y. Yu, Phys. Rev. E **78**, 066405 (2008).
[13] J. J. Drocco, L. M. Lopatina, C. Reichhardt, and C. J. Olson-Reichhardt, Proc. SPIE **8458**, 84581I (2012).
[14] H. J. Zhao, V. R. Misko, and F. M. Peeters, New J. Phys. **14**, 063032 (2012).
[15] V. A. Froltsov, R. Blaak, C. N. Likos, and H. Löwen, Phys. Rev. E **68**, 061406 (2003).
[16] H. Löwen, R. Messina, N. Hoffmann, C. E. C. N. Likos, P. Keim, U. Gasser, G. Maret, R. Goldberg, and T. Palberg, J. Phys.: Condens. Matter **17**, S3379 (2005).
[17] A. Reinmüller, E. C. Oguz, R. Messina, H. Löwen, H. J. Schöpe, and T. Palberg, Eur. Phys. J. Special Topics **222**, 3011 (2013).
[18] S. Deutschländer, T. Horn, H. Löwen, G. Maret, and P. Keim, Phys. Rev. Lett. **11**, 098301 (2013).
[19] H. Löwen, Eur. Phys. J. Special Topics **222**, 2727 (2013).
[20] V. Danilov, T. Prokopyeva, and S. Kantorovich, Phys. Rev. E **86**, 061408 (2012).
[21] S. Jager and S. H. L. Klapp, Phys. Rev. E **86**, 061402 (2012).
[22] D. Lucena, W. P. Ferreira, F. F. Munarin, G. A. Farias, and F. M. Peeters, Phys. Rev. E **87**, 012307 (2013).

[23] M. Knap, E. Berg, M. Ganahl, and E. Demler, Phys. Rev. B **86**, 064501 (2012).
[24] A. G. Volosniev, J. R. Armstrong, D. V. Fedorov, A. S. Jensen, and N. T. Zinner, Few-Body Syst. **54**, 707 (2013).
[25] B. Wunsch, N. T. Zinner, I. B. Mekhov, S. J. Huang, D. W. Wang, and E. Demler, Phys. Rev. Lett. **107**, 073201 (2011).
[26] J. Ruhman, E. G. Dalla-Torre, S. D. Huber, and E. Altman, Phys. Rev. B **85**, 125121 (2012).
[27] B. Spivak and S. A. Kivelson, Phys. Rev. B **70**, 155114 (2004).
[28] M. Bauer and M. M. Parish, Phys. Rev. Lett. **108**, 255302 (2012).
[29] Y. Yang, L. Gao, G. P. Lopez, and B. B. Yellen, ACS nano **7**, 2705 (2013).
[30] R. D. L. Hanes, C. Dalle-Ferrier, M. Scmiedeberg, M. C. Jenkins, and S. U. Egelhaaf, Soft Matter. **8**, 2714 (2012).
[31] J. C. N. Carvalho, K. Nelissen, W. P. Ferreira, G. A. Farias, and F. M. Peeters, Phys. Rev. E **85**, 021136 (2012).
[32] J. C. N. Carvalho, W. P. Ferreira, G. A. Farias, and F. M. Peeters, Phys. Rev. B **83**, 094109 (2011).
[33] T. Neuhaus, M. Schmiedeberg, and H. Löwen, New J. Phys. **15**, 073013 (2013).
[34] L. D. Carr, D. DeMille, R. V. Krems, and J. Ye, New. J. Phys. **11**, 055049 (2009).
[35] S. Herrera-Velarde and R. Castaneda-Priego, J. Phys.: Condens. Matter **19**, 226215 (2007).
[36] C. Reichhardt and C. J. Olson-Reichhardt, Phys. Rev. E **85**, 051401 (2012).
[37] C. Dalle-Ferrier, M. Kruger, R. D. L. Hanes, S. Walta, M. C. Jenkins, and S. U. Egelhaaf, Soft Matter. **7**, 2064 (2011).
[38] G. Piacente, G. Q. Hai, and F. M. Peeters, Phys. Rev. B **81**, 024108 (2010).
[39] T. Tlusty and S. A. safran, Science **290**, 1328 (2000).
[40] Y. Yang, L. Gao, G. P. Lopez, and B. B. Yellen, J. Chem. Phys. **135**, 034501 (2011).
[41] S. Roldán-Vargas, F. Smallenburg, W. Kob, and F. Sciortino, preprint cond-mat/1310.3730 (2013).
[42] M. A. Annunziata, A. M. Menzel, and H. Löwen, J. Chem. Phys. **138**, 204906 (2013).
[43] C. Bechinger, M. Brunner, and P. Leiderer, Phys. Rev. Lett. **86**, 930 (2001).